Average Current Mode Control of LLC Resonant Converter

| Author: | Dhaval Patel and Ramesh Kankanala Microchip Technology Inc. |

ABSTRACT

Average Current Mode Control (ACMC) of a Pulse-Frequency Modulated (PFM) LLC Resonant Converter considerably improves the dynamic response of the converter. ACMC also facilitates meeting current sharing requirements of parallel connected converters. A good control loop bandwidth is required to meet the dynamic response specifications and can be achieved using the ACMC-PFM LLC resonant converter. The plant transfer functions of the converter are derived using the Extended Describing Function (EDF), and appropriate compensators for the current and voltage control loops are designed. Experimental results verifying the model and design are presented and compared with the MATLAB® model results.

INTRODUCTION

In resonant converters, the operating principle is based on the characteristic gain curve of the resonant tank, where a change in the switching frequency will either increase or decrease the gain from the resonant tank. This results in an effective regulation of output voltage or current in relation to the load and input voltage changes. In the LLC resonant converter, the resonant tank is a set of two inductive elements and one capacitor (LLC).

The LLC resonant converter has several advantages over other traditional topologies. A few of them are as follows:
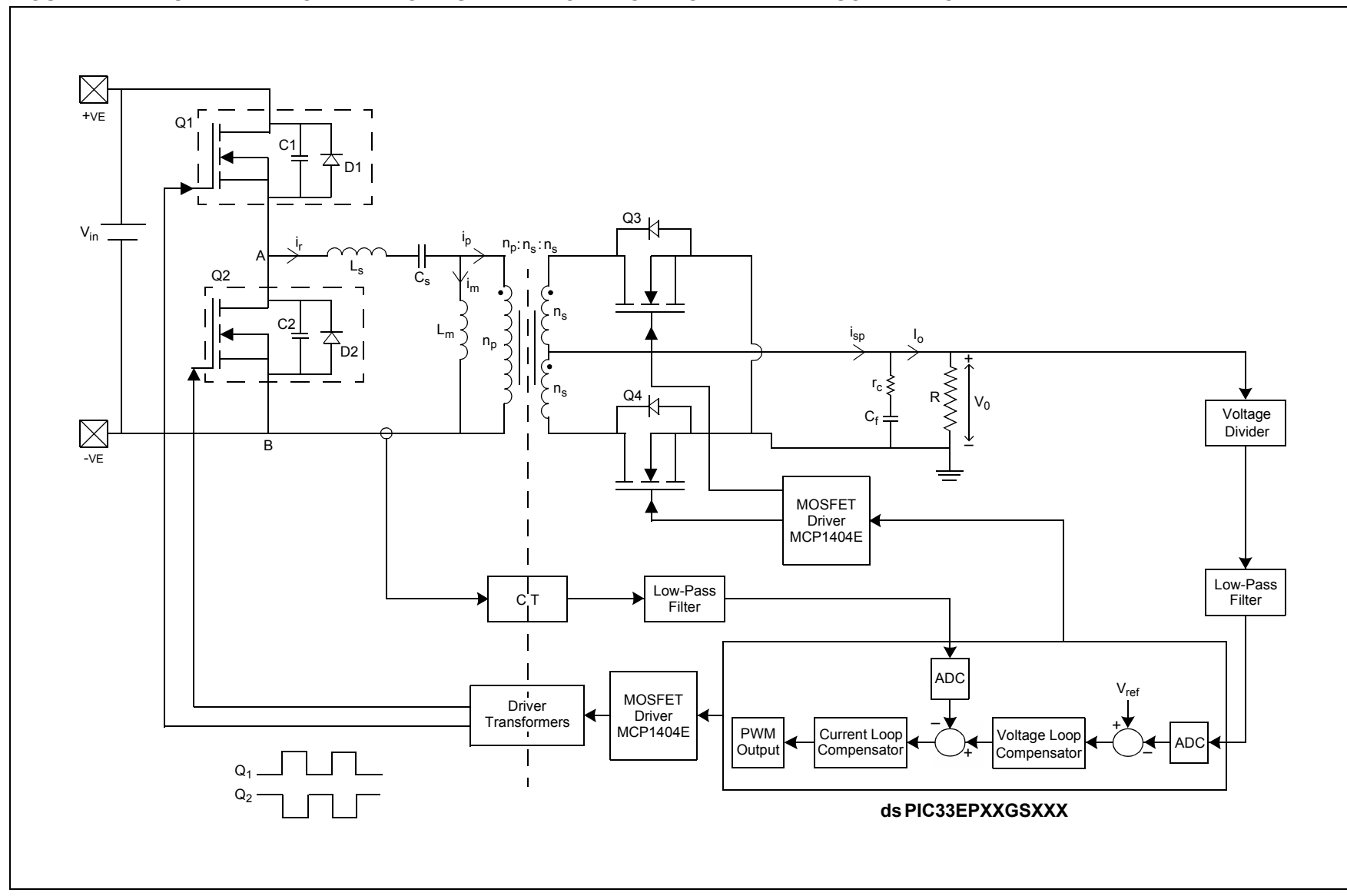
- LLC resonant converter can operate in both Step-up and Step-Down modes
- LLC resonant converter accommodates a wide range of output to input voltage ratios, with a relatively small frequency modulation range
- Zero Voltage Switching (ZVS) of primary MOSFETs could be achieved over the entire operating range and Zero Current Switching (ZCS) of secondary MOSFETs could be achieved over a specific operating range

The primary side of the ACMC-LLC resonant converter has a half-bridge configuration, and the secondary side of the transformer has a center-tapped full wave rectifier and capacitive filter (C_f). A simple capacitor filter is used instead of a standard LC filter, thereby reducing the cost, component count and converter dimensions. The Q_1 and Q_2 MOSFETs are driven in Complementary mode at 50% duty cycle (neglecting dead time). The resonant tank in the primary side of the converter has three passive components: magnetizing inductance (L_m), resonant capacitor (C_s) and series resonant inductor (L_s).

Modeling of the converter and compensator design for the ACMC-LLC resonant converter has been performed similar to the VMC-LLC resonant converter. Refer to *AN1477*, "*Digital Compensator Design for LLC Resonant Converter*" (DS00001477) for more information.

In order to develop the state-space model for the ACMC-LLC resonant converter, the linearized plant model equations are inherited from the equations derived in the document, *AN1477, "Digital Compensator Design for LLC Resonant Converter"*. This application note describes the mathematical modelling and digital compensator design for the ACMC-LLC resonant converter.

Figure 1 illustrates the ACMC-LLC resonant converter.

FIGURE 1: SCHEMATIC OF AVERAGE CURRENT MODE CONTROLLED LLC RESONANT CONVERTER

AVERAGE CURRENT MODE CONTROL VS. VOLTAGE MODE CONTROL

Current Mode Control (CMC) is a two-loop system, comprised of an inner current loop and an outer voltage loop (see Figure 1). The CMC method is widely used in Pulse-Width Modulation (PWM) converters and has the following advantages:

- Improved transient response: A CMC converter can be typically modeled as a first order system. Hence, it is easier to design a feedback network, and further, the overall transient response is improved.

- Improved disturbance rejection: The output of the constant current converter is nearly independent of variations in input voltage. This is achieved by a fast acting inner current loop which tightly controls the load current.

- Suitability for modular operation: When multiple converters are paralleled in an input-parallel/output-parallel combination, a common outer voltage feedback loop is sufficient for all paralleled converters. This configuration automatically enables equal or weighted load sharing through a common current reference for the individual inner current loops. The paralleled converters have the same control voltage, so there is equal load sharing.

- Self-protection against overload: The ACMC converter incorporates overload protection through the provision of limit checks to the current reference for the inner current loop.

- Transformer anti-saturation control: The current threshold control algorithm (inner current loop) automatically limits the maximum current through the transformer windings, thereby keeping the operating point of the transformer near the center of its B-H curve.

ACMC is implemented by sensing the resonant tank current (i_r in Figure 1) using a current-sensing network (CT) and a low-pass filter. This sensed current is fed to the current loop compensator. The reference to the inner current loop compensator is obtained from the output of the outer voltage loop compensator. The output of the current compensator defines the required operating frequency to be programmed to the PWM generator (PTPER register) for controlling the primary side MOSFETs of the half-bridge.

Plant Transfer Function

The plant transfer functions of the LLC resonant converter are derived using the EDFs. As mentioned in the **"Introduction"**, the modeling of the converter and compensator design for the ACMC-LLC resonant converter has been performed similar to the VMC-LLC resonant converter. Refer to the application note, *AN1477, "Digital Compensator Design for LLC Resonant Converter"*, for deriving the large signal model of the LLC resonant converter.
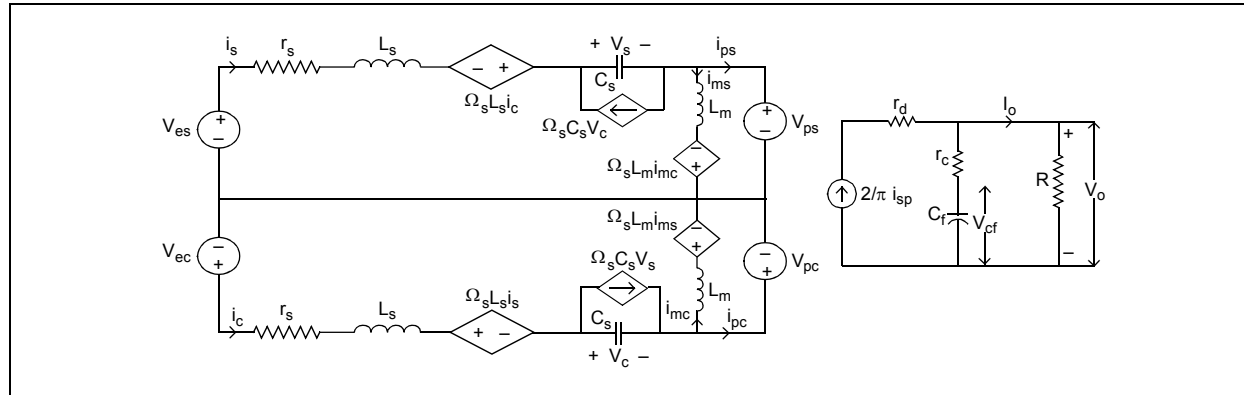
The large signal model of the LLC resonant converter is provided in Equation 1.

EQUATION 1: LARGE SIGNAL MODEL OF LLC RESONANT CONVERTER

$$v_{es} = L_s\left(\frac{di_s}{dt} + \omega_s i_c\right) + r_s i_s + v_s + \frac{4n}{\pi}\frac{i_{ps}}{i_{pp}}abs(v_{se})$$

$$v_{ec} = 0 = L_s\left(\frac{di_c}{dt} - \omega_s i_s\right) + r_s i_c + v_c + \frac{4n}{\pi}\frac{i_{pc}}{i_{pp}}abs(v_{se})$$

$$i_s = C_s\left(\frac{dv_s}{dt} + \omega_s v_c\right)$$

$$i_c = C_s\left(\frac{dv_c}{dt} - \omega_s v_s\right)$$

$$L_m\left(\frac{di_{ms}}{dt} + \omega_s i_{mc}\right) = \frac{4n}{\pi}\frac{i_{ps}}{i_{pp}}abs(v_{se}) = v_{ps}$$

$$L_m\left(\frac{di_{mc}}{dt} - \omega_s i_{ms}\right) = \frac{4n}{\pi}\frac{i_{pc}}{i_{pp}}abs(v_{se}) = v_{pc}$$

$$\left(1 + \frac{r_c}{R}\right)C_f\frac{dv_{c_f}}{dt} + \frac{1}{R}v_{c_f} = \frac{2}{\pi}i_{sp}$$

$$v_0 = \frac{2}{\pi}r'_c i_{sp} + \left(\frac{r'_c}{r_c}\right)v_{c_f}$$

An equivalent circuit representation of the large signal model of the LLC resonant converter is illustrated in Figure 2.

AN1495

FIGURE 2: LARGE SIGNAL MODEL OF LLC RESONANT CONVERTER

The following variables are used in the large signal model:

- i_s and i_c: Sine and cosine components of the resonant inductor current

- i_{ms} and i_{mc}: Sine and cosine components of the magnetizing current

- V_s and V_c: Sine and cosine components of the resonant capacitor voltage

- V_{es} and V_{ec}: Sine and cosine components of the half-bridge output voltage

- V_{ps} and V_{pc}: Sine and cosine components of the transformer primary voltage

- i_{ps} and i_{pc}: Sine and cosine components of the transformer primary current

- i_p and r_s: Transformer primary current and DCR of the resonant inductor

- i_{sp} and V_{cf}: Transformer secondary current and output filter capacitor voltage

- Ω_s and V_o: Steady-state switching frequency and output voltage

- C_f and r_c: Output filter capacitor and filter capacitor Equivalent Series Resistance (ESR)

- R and I_o: Load resistance and load current

The large signal model of the LLC resonant converter, provided in Equation 1, is perturbed and linearized about the chosen operating point to obtain small signal model equations. These equations are used to determine the plant transfer functions, such as output voltage-to-switching frequency ($G_{v\omega}(s)$) and resonant inductor current-to-switching frequency ($G_{i\omega}(s)$) for ACMC.

The difference between the state-space models of VMC and ACMC is the presence of an additional output variable, which is the average inductor current (i_r) in the ACMC model.

The perturbation and linearization of the resonant inductor current are provided in Equation 2.

EQUATION 2: PERTURBATION AND LINEARIZATION OF RESONANT INDUCTOR CURRENT

$$i_r = \sqrt{i_s^2 + i_c^2}$$

$$i_{r,avg} = \frac{2}{\pi} i_r$$

Linearization of the Tank Current is:

$$\hat{i}_{r,avg} = \frac{2}{\pi}\frac{I_s}{\sqrt{I_s^2 + I_c^2}}\hat{i}_s + \frac{2}{\pi}\frac{I_c}{\sqrt{I_s^2 + I_c^2}}\hat{i}_c = J_s\hat{i}_s + J_c\hat{i}_c$$

Where:

$$J_s = \frac{2}{\pi}\frac{I_s}{\sqrt{I_s^2 + I_c^2}}$$

$$J_c = \frac{2}{\pi}\frac{I_c}{\sqrt{I_s^2 + I_c^2}}$$

The linearized small signal model of the LLC resonant converter for ACMC is provided in Equation 3. Equation 3 incorporates the linearized resonant current, as derived in Equation 2.

EQUATION 3:   LINEARIZED SMALL SIGNAL MODEL OF LLC RESONANT CONVERTER

$$\frac{d\hat{i}_s}{dt} = -\left(\frac{H_{ip}+r_s}{L_s}\right)\hat{i}_s - \left(\frac{\Omega_s L_s + H_{ic}}{L_s}\right)\hat{i}_c - \frac{1}{L_s}\hat{v}_s + \frac{H_{ip}}{L_s}\hat{i}_{ms} + \frac{H_{ic}}{L_s}\hat{i}_{mc} - \frac{H_{vcf}}{L_s}\hat{v}_{cf} + \frac{K_1}{L_s}\hat{v}_{in} + \frac{K_2}{L_s}\hat{d} - \frac{L_s\omega_0 I_c}{L_s}\hat{\omega}_{sn}$$

$$\frac{d\hat{i}_c}{dt} = \frac{(\Omega_s L_s - G_{ip})}{L_s}\hat{i}_s - \frac{(G_{ic}+r_s)}{L_s}\hat{i}_c - \frac{1}{L_s}\hat{v}_c + \frac{G_{ip}}{L_s}\hat{i}_{ms} + \frac{G_{ic}}{L_s}\hat{i}_{mc} - \frac{G_{vcf}}{L_s}\hat{v}c_f + \frac{L_s\omega_0 I_s}{L_s}\hat{\omega}_{sn}$$

$$\frac{d\hat{v}_s}{dt} = \frac{1}{C_s}\hat{i}_s - \frac{C_s\Omega_s}{C_s}\hat{v}_c - \frac{C_s\omega_0 V_c}{C_s}\hat{\omega}_{sn}$$

$$\frac{d\hat{v}_c}{dt} = \frac{1}{C_s}\hat{i}_c + \frac{C_s\Omega_s}{C_s}\hat{v}_s + \frac{C_s\omega_0 V_s}{C_s}\hat{\omega}_{sn}$$

$$\frac{d\hat{i}_{ms}}{dt} = \frac{H_{ip}}{L_m}\hat{i}_s + \frac{H_{ic}}{L_m}\hat{i}_c - \frac{H_{ip}}{L_m}\hat{i}_{ms} - \frac{(H_{ic}+L_m\Omega_s)}{L_m}\hat{i}_{mc} + \frac{H_{vcf}}{L_m}\hat{v}c_f - \frac{L_m I_{mc}\omega_0}{L_m}\hat{\omega}_{sn}$$

$$\frac{d\hat{i}_{mc}}{dt} = \frac{G_{ip}}{L_m}\hat{i}_s + \frac{G_{ic}}{L_m}\hat{i}_c - \frac{(G_{ip}-L_m\Omega_s)}{L_m}\hat{i}_{ms} - \frac{G_{ic}}{L_m}\hat{i}_{mc} + \frac{G_{vcf}}{L_m}\hat{v}c_f + \frac{L_m I_{ms}\omega_0}{L_m}\hat{\omega}_{sn}$$

$$\frac{d\hat{V}_{cf}}{dt} = \frac{K_{is}r'_c}{C_f r_c}\hat{i}_s + \frac{K_{ic}r'_c}{C_f r_c}\hat{i}_c - \frac{K_{is}r'_c}{C_f r_c}\hat{i}_{ms} - \frac{K_{ic}r'_c}{C_f r_c}\hat{i}_{mc} - \frac{r'_c}{RC_f r_c}\hat{v}_{cf}$$

The Output Equation is:

$$\hat{v}_0 = K_{is}r'_c\hat{i}_s + K_{ic}r'_c\hat{i}_c - K_{is}r'_c\hat{i}_{ms} - K_{ic}r'_c\hat{i}_{mc} + \left(\frac{r'_c}{r_c}\right)\hat{v}_{cf}$$

$$\hat{i}_{r,avg} = J_s\hat{i}_s + J_c\hat{i}_c$$

Where:

$$H_{ip} = \frac{4nV_{cf}}{\pi}\left(\frac{r'_c}{r_c}\right)\frac{I_{pc}^2}{I_{pp}^3} + \frac{8n^2}{\pi^2}(r_d+r'_c)$$

$$H_{ic} = -\frac{4nV_{cf}}{\pi}\left(\frac{r'_c}{r_c}\right)\frac{I_{ps}I_{pc}}{I_{pp}^3}$$

$$H_{vcf} = \frac{4n}{\pi}\left(\frac{r'_c}{r_c}\right)\frac{I_{ps}}{I_{pp}}$$

$$G_{ip} = -\frac{4nV_{cf}}{\pi}\left(\frac{r'_c}{r_c}\right)\frac{I_{ps}I_{pc}}{I_{pp}^3}$$

$$G_{ic} = \frac{4nV_{cf}}{\pi}\left(\frac{r'_c}{r_c}\right)\frac{I_{ps}^2}{I_{pp}^3} + \frac{8n^2}{\pi^2}(r_d+r'_c)$$

$$G_{vcf} = \frac{4n}{\pi}\left(\frac{r'_c}{r_c}\right)\frac{I_{pc}}{I_{pp}}$$

$$K_1 = \frac{2}{\pi}\sin\left(\frac{\pi}{2}D\right)$$

$$K_2 = V_{in}\cos\left(\frac{\pi}{2}D\right)$$

$$K_{is} = \frac{2n}{\pi}\frac{I_{ps}}{\sqrt{I_{ps}^2+I_{pc}^2}}$$

$$K_{ic} = \frac{2n}{\pi}\frac{I_{pc}}{\sqrt{I_{ps}^2+I_{pc}^2}}$$

Formation of State-Space Model

State-space representation is a mathematical model of a physical system as a set of input, output and state variables, related by first order differential equations.

The state-space representation (known as time domain approach) provides a convenient and compact way to model and analyze systems with multiple inputs and outputs.

The linearized model obtained in Equation 3 is transformed into the state-space representation. The state-space model is used to obtain the transfer functions between output voltage and switching frequency ($G_{v\omega}(s)$), and between inductor current and switching frequency ($G_{i\omega}(s)$).

Equation 4 provides the state-space representation of the ACMC-LLC resonant converter.

EQUATION 4:   STATE-SPACE MODEL OF LLC RESONANT CONVERTER

$$\frac{d\hat{x}}{dt} = A\hat{x} + B\hat{u}$$

$$\hat{y} = C\hat{x} + D\hat{u}$$

Where:

$$\hat{x} = \begin{bmatrix} \hat{i}_s & \hat{i}_c & \hat{v}_s & \hat{v}_c & \hat{i}_{ms} & \hat{i}_{mc} & \hat{v}_{c_f} \end{bmatrix}^T \quad \text{States of the System}$$

$$\hat{u} = \begin{bmatrix} \hat{f}_{sn} & or & \hat{\omega}_{sn} \end{bmatrix} \quad \text{Control Inputs and All Other Disturbance Inputs are Ignored}$$

$$\hat{y} = \begin{bmatrix} \hat{v}_o \\ \hat{i}_{r,avg} \end{bmatrix} \quad \text{Outputs}$$

$$A = \begin{bmatrix}
-\dfrac{H_{ip}+r_s}{L_s} & -\dfrac{(\Omega_s L_s + H_{ic})}{L_s} & -\dfrac{1}{L_s} & 0 & \dfrac{H_{ip}}{L_s} & \dfrac{H_{ic}}{L_s} & -\dfrac{H_{vcf}}{L_s} \\[2ex]
\dfrac{\Omega_s L_s - G_{ip}}{L_s} & -\dfrac{G_{ic}+r_s}{L_s} & 0 & -\dfrac{1}{L_s} & \dfrac{G_{ip}}{L_s} & \dfrac{G_{ic}}{L_s} & -\dfrac{G_{vcf}}{L_s} \\[2ex]
\dfrac{1}{C_s} & 0 & 0 & -\dfrac{C_s \Omega_s}{C_s} & 0 & 0 & 0 \\[2ex]
0 & \dfrac{1}{C_s} & \dfrac{C_s \Omega_s}{C_s} & 0 & 0 & 0 & 0 \\[2ex]
\dfrac{H_{ip}}{L_m} & \dfrac{H_{ic}}{L_m} & 0 & 0 & -\dfrac{H_{ip}}{L_m} & -\dfrac{H_{ic}+L_m\Omega_s}{L_m} & \dfrac{H_{vcf}}{L_m} \\[2ex]
\dfrac{G_{ip}}{L_m} & \dfrac{G_{ic}}{L_m} & 0 & 0 & -\dfrac{G_{ip}-L_m\Omega_s}{L_m} & -\dfrac{G_{ic}}{L_m} & \dfrac{G_{vcf}}{L_m} \\[2ex]
\dfrac{K_{is}r'_c}{C_f r_c} & \dfrac{K_{ic}r'_c}{C_f r_c} & 0 & 0 & -\dfrac{K_{is}r'_c}{C_f r_c} & -\dfrac{K_{ic}r'_c}{C_f r_c} & -\dfrac{r'_c}{RC_f r_c}
\end{bmatrix}$$

$$B = \begin{bmatrix} (-\omega_0 I_c) & (\omega_0 I_s) & (-\omega_0 V_c) & (\omega_0 V_s) & (-\omega_0 I_{mc}) & (\omega_0 I_{ms}) & 0 \end{bmatrix}$$

$$C = \begin{bmatrix} (K_{is}\,r'_c) & (K_{ic}r'_c) & 0 & 0 & (-K_{is}\,r'_c) & (-K_{ic}\,r'_c) & \left(\dfrac{r'_c}{r_c}\right) \\[2ex] J_s & J_c & 0 & 0 & 0 & 0 & 0 \end{bmatrix}$$

$$D = \begin{bmatrix} 0 \\ 0 \end{bmatrix}$$

From the state-space model in Equation 4, the control-to-output voltage transfer function ($G_{v\omega}(s)$) and the control-to-inductor current transfer function ($G_{i\omega}(s)$) are provided in Equation 5, where the control variable is the PWM switching frequency of an LLC resonant converter.

EQUATION 5: **($G_{i\omega}(s)$) AND ($G_{v\omega}(s)$) TRANSFER FUNCTIONS**

$$\begin{bmatrix} \hat{v}_0 / \hat{\omega}_{sn} \\ \hat{i}_r / \hat{\omega}_{sn} \end{bmatrix} = C(sI-A)^{-1}B + D = \begin{bmatrix} G_{v\omega}\ (s) \\ G_{i\omega}\ (s) \end{bmatrix}$$

Equation 5 is solved in order to obtain the $G_{v\omega}(s)$ and $G_{i\omega}(s)$ transfer functions.

HARDWARE DESIGN SPECIFICATIONS

Series Resonant Inductor (L_s) = 62 µH

Series Resonant Capacitance (C_s) = 9.4 nF

Magnetizing Inductor (L_m) = 268 µH

Input Voltage (V_{in}) = 400V (DC)

Output Filter Capacitance (C_f) = 5 x 330 µF

Output Power = 200W

Switching Frequency (f_s) = 200 kHz

DC Resistance (DCR) of Resonant Inductor (r_s) = 15 mΩ

ESR of Output Capacitor (r_c) = 15 mΩ

Transformer Turns Ration (n) = 17

Secondary MOS Resistor (r_d) = 0.725 mΩ

Equation 1 provides the MATLAB commands to obtain the $G_{v\omega}(s)$ and $G_{i\omega}(s)$ transfer functions.

EXAMPLE 1: **MATLAB® COMMANDS**

```
sys=ss(A,B,C,D);      % arranges the A,B,C,D
matrices into a state-space model
H=tf(sys);            % Plant transfer functions
```

PLANT TRANSFER FUNCTION

After solving Equation 5, using Example 1 with the hardware design specifications, $G_{i\omega}(s)$ and $G_{v\omega}(s)$ are provided in Equation 6 and Equation 7. In resonant converters, the poles and zeros are the functions of the normalized switching frequency ($\omega_{sn} = \omega_s / \omega_0$). Where, ω_s = switching frequency and ω_0 = resonant frequency.

Equation 6 and Equation 7 are obtained after neglecting the poles and zeros above the switching frequency (ω_s).

EQUATION 6: **INDUCTOR CURRENT-TO-SWITCHING FREQUENCY TRANSFER FUNCTION**

$$G_{i\omega}(s) = \frac{0.8715 \times \left(\frac{s}{1499} + 1\right)}{\left(\frac{s^2}{(3.0798 \times 10^4)^2} + \frac{1.3365s}{3.0798 \times 10^4} + 1\right)\left(\frac{s^2}{(1.05 \times 10^6)^2} + \frac{0.2568s}{1.05 \times 10^6} + 1\right)}$$

The General Form of $G_{i\omega}(s)$:

$$G_{i\omega}(s) = \frac{G_{co} \times \left(1 + \frac{s}{\omega_{esr}}\right)}{\left(\frac{s^2}{\omega_{p1}^2} + \frac{s}{(Q_1 \cdot \omega_{p1})} + 1\right) \times \left(\frac{s^2}{\omega_{p2}^2} + \frac{s}{(Q_2 \cdot \omega_{p2})} + 1\right)}$$

EQUATION 7: **OUTPUT VOLTAGE-TO-SWITCHING FREQUENCY TRANSFER FUNCTION**

$$G_{v\omega}(s) = \frac{6.4285 \times \left(\frac{s}{2.367 \times 10^5} + 1\right) \times \left(\frac{s}{6.711 \times 10^5} - 1\right)}{\left(\frac{s^2}{(3.0798 \times 10^4)^2} + \frac{1.3365s}{3.0798 \times 10^4} + 1\right)\left(\frac{s^2}{(1.05 \times 10^6)^2} + \frac{0.2568s}{1.05 \times 10^6} + 1\right)}$$

## Digital Compensator Design for ACMC-LLC Resonant Converter
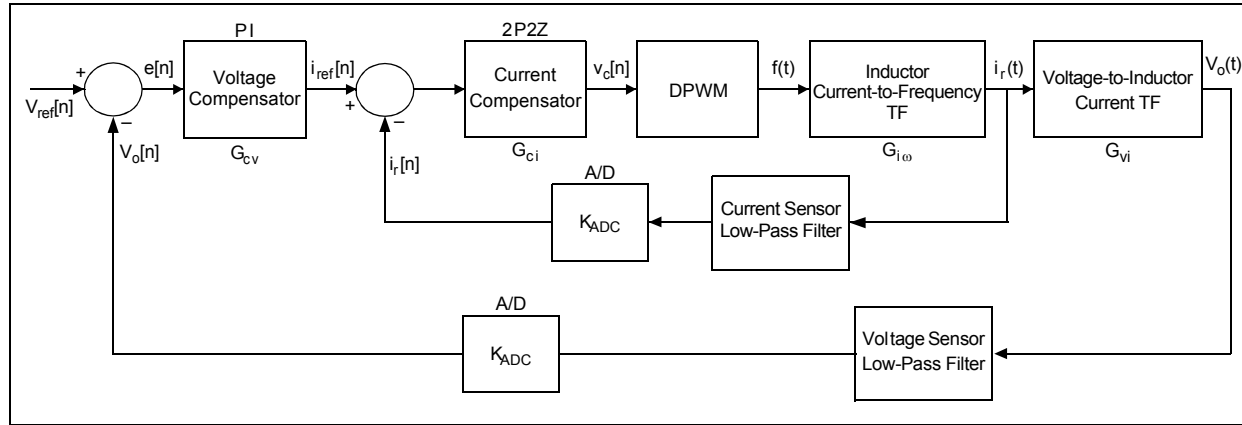
The ACMC-LLC resonant converter control system is comprised of two loops: an inner current loop and an outer voltage loop, as illustrated in Figure 3. The inner current loop directly controls the inductor current. The output of the inner current loop defines the frequency of the PWM module to drive the half-bridge MOSFETs. The outer voltage loop controls the output voltage by generating the current reference for the inner current loop. To ensure stable operation of the multiloop converter, all the sequential loops in the circuit should be stable with a sufficient degree of stability.

The digital compensator is designed for the plant transfer functions, as obtained in Equation 6. For stable operation of a multiloop control system, the inner current loop must be faster than the outer voltage loop.

In order to achieve a higher bandwidth for the inner current loop, and satisfy the gain margin and phase margin stability requirements, a digital 2-Pole 2-Zero (2P2Z) compensator has been chosen. A digital PI compensator has been chosen for the outer voltage loop.

The digital compensators have been derived using the design by emulation or digital redesign approach. In this approach, the compensator is designed in the continuous time domain and then converted to discrete time domain using the Bilinear or Tustin transformation.

FIGURE 3: CONTROL LOOP BLOCK DIAGRAM OF ACMC-LLC RESONANT CONVERTER
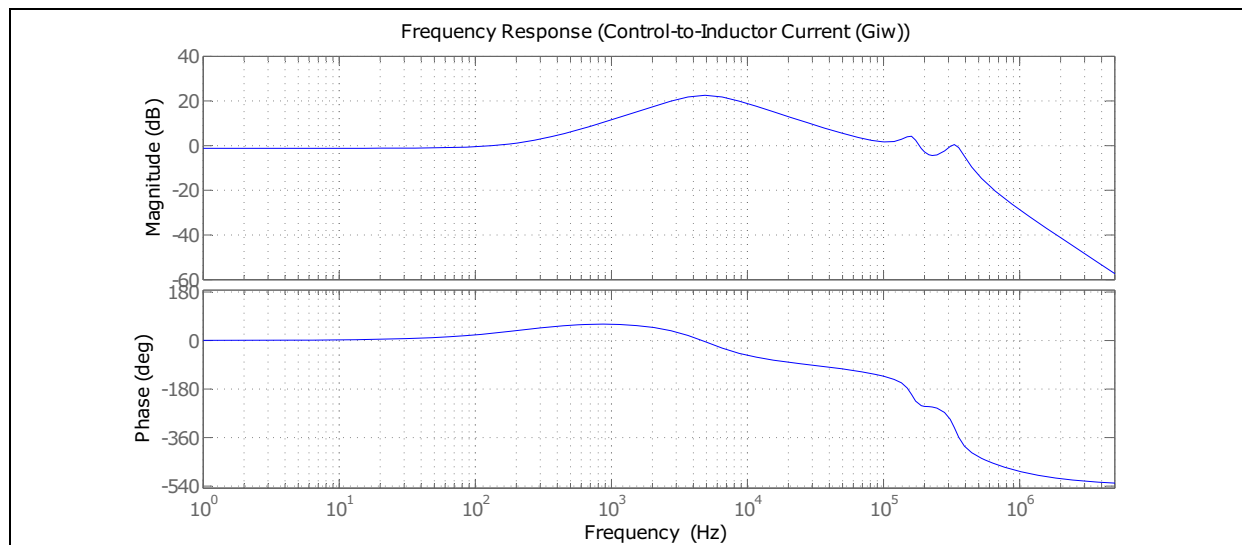
Inner Current Loop

The inner current loop compensator is designed to control the frequency to inductor current transfer function of the converter ($G_{i\omega}(s)$). The inner current loop ($V_c[n]$) directly controls the inductor current.
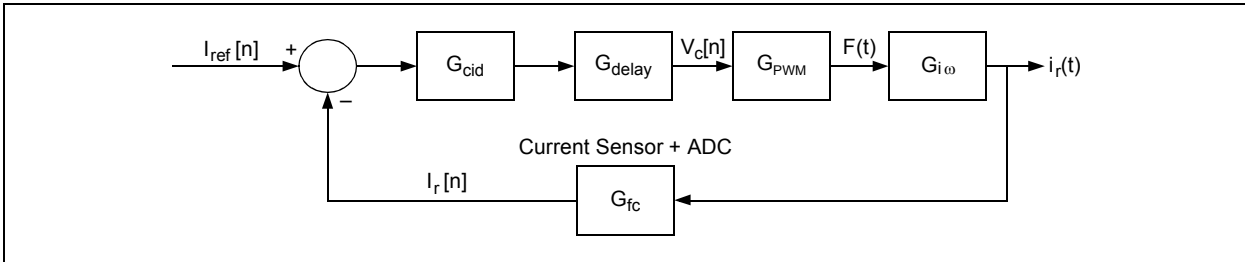
The output of the inner current loop defines the frequency of the PWM module output to drive the half-bridge MOSFETs. The frequency response of Equation 6 is illustrated in Figure 4.

FIGURE 4: FREQUENCY RESPONSE OF INDUCTOR CURRENT-TO-SWITCHING FREQUENCY TRANSFER FUNCTION

The control block diagram for the inner current loop, including the low-pass filter (G_{fc}), computation and digital delay (G_{delay}), digital 2-Pole 2-Zero (2P2Z) (G_{ci}) compensator and PWM (G_{PWM}) is illustrated in Figure 5.

FIGURE 5:   CONTROL BLOCK DIAGRAM OF INNER CURRENT LOOP

A first order low-pass filter (G_{fc}) is provided to filter the resonant tank current using a current transformer or any other current-sensing network. The low-pass filter transfer function is provided in Equation 8.

EQUATION 8:   CURRENT SENSOR NETWORK LOW-PASS FILTER TRANSFER FUNCTION

$$G_{fc}(s) = \frac{1}{(R_{fc}C_{fc}s + 1)}$$

Where:
LPF Resistor: $R_{fc} = 10\,\Omega$
LPF Capacitor: $C_{fc} = 2\,\mu F$

The inductor current to switching frequency plant transfer function, provided in Equation 6, consists of a low-frequency zero and a pair of dominant complex poles. The low-frequency zero mainly depends on the output filter capacitor value. The effect of this low-frequency zero increases gain at high frequency. To compensate for this effect, a pole (ω_p) is included in the compensator. In order to minimize the steady-state error, an integrator (K_{ci}) is added to the compensator.

To compensate for reduction in system damping, and hence, increased overshoots, increased settling time due to the effect of the complex dominant poles, two zeros ($s+\alpha+j\beta$) and ($s+\alpha-j\beta$) are added.

Apart from this, the low-pass current sense filter adds a pole at comparatively lower frequency, as seen in Equation 8. The main reason to use a heavy low-pass filter at current sense is to get an average value from the rectified sinusoidal tank current of the switching frequency.

Effectively, the inner current loop control system will have a 2-Pole 2-Zero in the continuous domain, as provided in Equation 9. A simple pole/zero placement method is adopted here for designing the controller.

EQUATION 9:   COMPENSATOR ($G_{ci}(s)$) IN CONTINUOUS TIME DOMAIN

$$G_{ci}(s) = \frac{K_{ci} \times \left(\frac{s}{\omega_{z1}} + 1\right) \times \left(\frac{s}{\omega_{z2}} + 1\right)}{s \times \left(\frac{s}{\omega_p} + 1\right)}$$

Based on the observation of Bode plots of plant and current sense filter, the compensator pole, ω_p ($2\pi f_p$), is placed at 24.37k radians/second to compensate for the effect of plant zero. Two real zeros are included in the compensator transfer function at locations, ω_{z1} = 28.05k and ω_{z2} = 50k radians/second, to provide the necessary phase lead. K_{ci} represents the integrator gain of the compensator and is adjusted to achieve the desired crossover frequency of the converter. In this analysis, computation and digital delay, and PWM gain, are assumed to be unity.

The desired crossover frequency is f_{ci} in Hz and $\omega_{ci} = j2\pi f_{ci}$ in radians/second. At crossover frequency, the loop gain of the system should be 0 dB or one in linear scale. The inner current loop compensator gain calculation is provided in Equation 10.

EQUATION 10:   INNER CURRENT LOOP COMPENSATOR GAIN CALCULATION

$$G_{i\omega}(s)\big|_{s\,=\,\omega_{ci}} \times G_{ci}(s)\big|_{s\,=\,\omega_{ci}} = 1$$

The Required Gain of the Compensator is:

$$K_{ci} = \frac{1}{G_{i\omega}(s)\big|_{s\,=\,\omega_{ci}} \times G_{ci}(s)\big|_{s\,=\,\omega_{ci}}}$$

AN1495

The low-pass current sense filter imposes some limitation on selection of crossover frequency. The corner frequency of this filter, based on Equation 8 parameters, is 50k radian/second (~8 kHz). Hence, the crossover frequency of the inner loop gain is chosen at 5 kHz. The required phase margin of the inner loop compensator is ~70 degrees to get a better stability margin. The resulting compensator for achieving a crossover frequency of ~5 kHz and a phase margin of 70 degrees is provided in Equation 11.

EQUATION 11:   INNER CURRENT LOOP COMPENSATOR TRANSFER FUNCTION ($G_{ci}(s)$)

$$G_{ci}(s) = \frac{0.13037 \times (s^2 + 7.805 \times 10^4 s + 1.4025 \times 10^9)}{s(s + 2.437 \times 10^4)}$$

The inner current loop gain is the product of gains around the forward path and feedback path of the loop, as provided in Equation 12. Equation 12 shows how the addition of a feedback loop modifies the transfer functions and performance of the inner current loop.

EQUATION 12:   INNER CURRENT LOOP GAIN

$$Inner\ Current\ Loop\ Gain\ =\ G_{fc}(s) \times G_{ci}(s) \times G_{delay}(s) \times G_{PWM}(s) \times G_{i\omega}(s)$$

Where:

$G_{delay}(s)$ = Transfer Functions of Transportation Delay
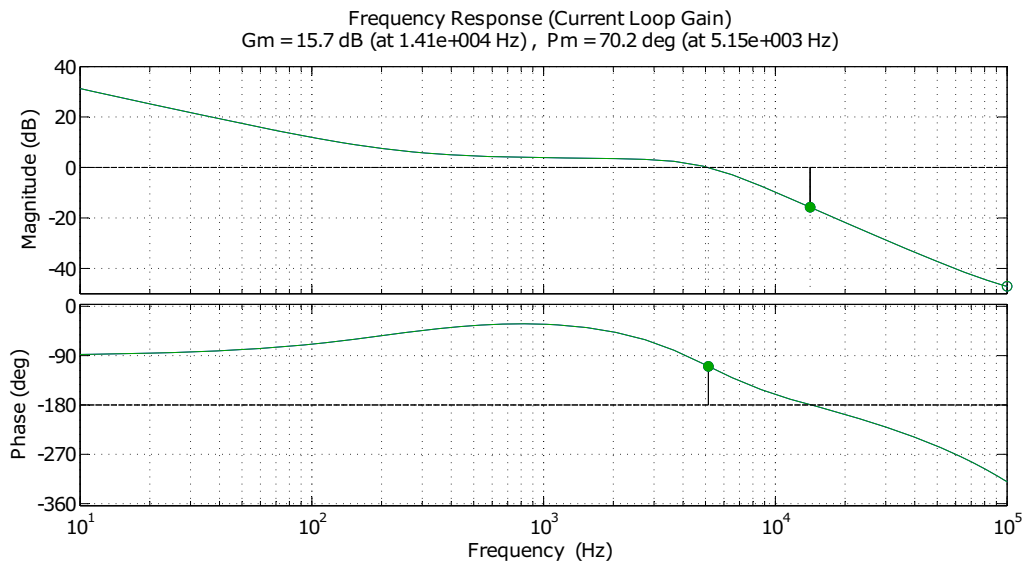
$G_{ci}(s)$ = Transfer Function of the Inner Current Loop Compensator

$G_{fc}(s)$ = Current Sensor Network Low-Pass Filter

$G_{PWM}(s)$ = PWM Module Gain

Frequency response of the inner current loop gain in Equation 12 is illustrated in Figure 6, where the crossover frequency is ~5 kHz.

FIGURE 6:   FREQUENCY RESPONSE PLOT OF LOOP GAIN (INNER CURRENT LOOP)

© 2013-2019 Microchip Technology Inc.

The continuous domain, 2-Pole 2-Zero (2P2Z) compensator in Equation 11 is converted to z-domain using the Tustin or Bilinear transformation, where $s = 2/T_s \ [(z-1)/(z+1)]$ with a sampling frequency of 200 kHz. The z-domain compensator transfer function ($G_{cid}(z)$) is provided in Equation 13.
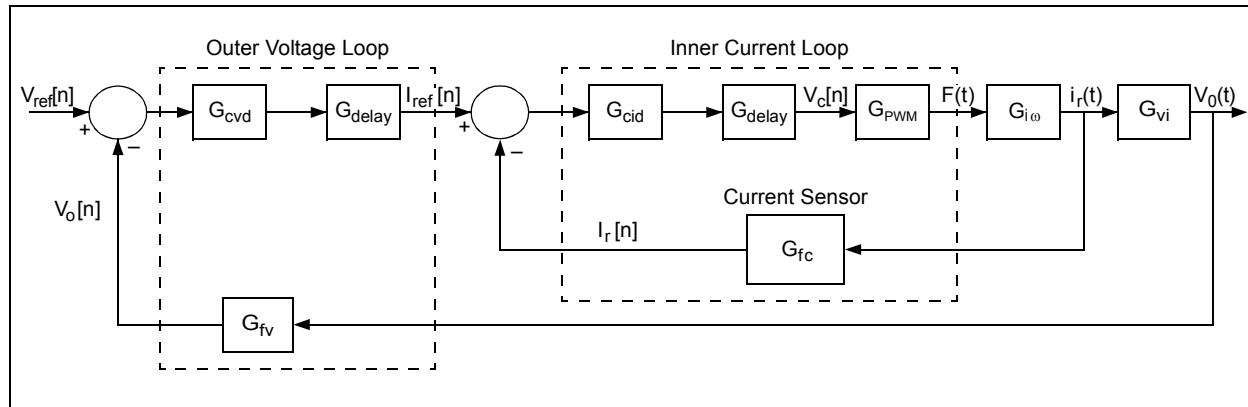
EQUATION 13: INNER CURRENT LOOP COMPENSATOR TRANSFER FUNCTION IN DISCRETE DOMAIN ($G_{cid}(z)$)

$$G_{cid}(z) = \frac{0.1479z^2 - 0.2436z + 0.09998}{z^2 - 1.885z + 0.8851}$$

FIGURE 7: CONTROL SYSTEM BLOCK DIAGRAM OF OUTER VOLTAGE LOOP

From Figure 7, it is clear that the closed-loop transfer function of the inner current loop is necessary to obtain the frequency response of the outer voltage loop. The closed-loop transfer function of inner current loop (G_{iCL}) is provided in Equation 14 and this includes the transfer function of the forward path and feedback path.

EQUATION 14: CLOSED-LOOP TRANSFER FUNCTION OF INNER CURRENT LOOP ($G_{iCL}(s)$)

$$G_{iCL}(s) = \frac{i_r(s)}{i_{ref}(s)}$$

$$= \frac{G_{ci}(s) \times G_{delay}(s) \times G_{PWM}(s) \times G_{i\omega}(s)}{1 + G_{fc}(s) \times G_{ci}(s) \times G_{delay}(s) \times G_{PWM}(s) \times G_{i\omega}(s)}$$

For the outer voltage loop, the plant transfer function will be the inductor current-to-output voltage transfer function ($G_{vi}(s)$), as provided in Equation 15.

Outer Voltage Loop

The outer voltage loop controls the output voltage (V_o) by generating a current reference ($I_{ref}(n)$) for the inner current loop. To ensure stable operation of the multi-loop converter, all the sequential loops (inner current loop in this application) in the circuit should be stable with sufficient stability. The outer voltage loop control system block diagram is illustrated in Figure 7.

EQUATION 15: INDUCTOR CURRENT-TO-OUTPUT VOLTAGE TRANSFER FUNCTION ($G_{vi}(s)$)

$$G_{vi}(s) = \frac{G_{v\omega}(s)}{G_{i\omega}(s)}$$

$$G_{vi}(s) = \frac{7.5471 \times \left(\frac{s}{2.367 \times 10^5} + 1\right)\left(\frac{s}{6.711 \times 10^5} - 1\right)}{\left(\frac{s}{1499} + 1\right)}$$

A first order low-pass filter has been used for filtering high-frequency noise from the output voltage measurement. This filter transfer function is provided in Equation 16.

EQUATION 16: LOW-PASS FILTER TRANSFER FUNCTION ($G_{fv}(s)$)

$$G_{fv}(s) = \frac{1}{(R_{fv}C_{fv}s + 1)}$$

Where:
LPF Resistor: R_{fv} = 1153Ω
LPF Capacitor: C_{fv} = 2000 pF

AN1495

The outer voltage loop gain is the product of gains around the forward path and feedback path of the loop and is provided in Equation 17, and this includes the closed-loop transfer function of the inner current loop.
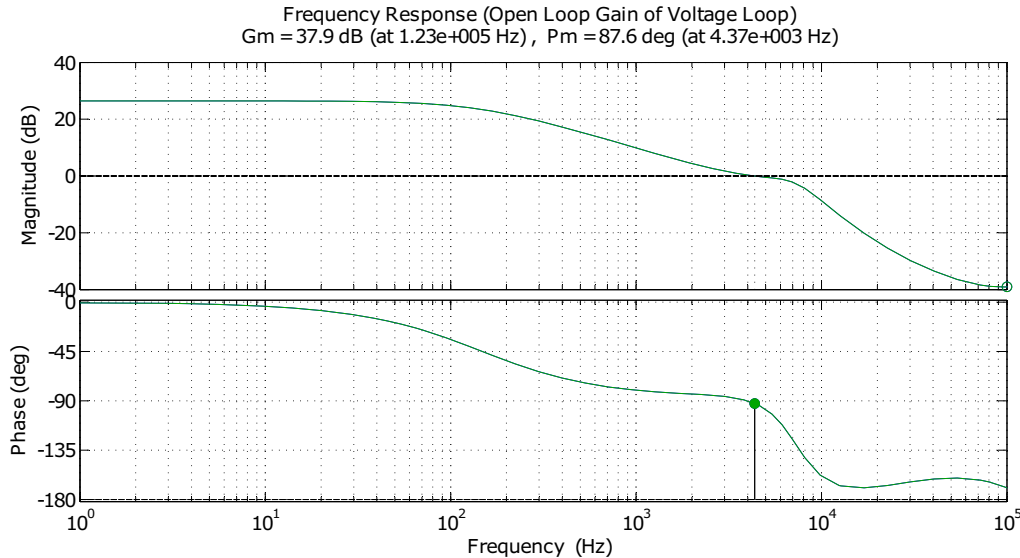
EQUATION 17: OPEN-LOOP GAIN OF OUTER VOLTAGE LOOP ($G_{vl}(s)$)

Open-Loop Gain of the Outer Voltage Loop:

$$G_{vl}(s) = G_{delay}(s) \times G_{iCL}(s) \times G_{vi}(s)$$

Open-loop gain of the outer voltage loop frequency response is illustrated in Figure 8.

FIGURE 8: FREQUENCY RESPONSE OF OPEN-LOOP GAIN OF OUTER VOLTAGE LOOP

Frequency Response (Open Loop Gain of Voltage Loop)
Gm = 37.9 dB (at 1.23e+005 Hz), Pm = 87.6 deg (at 4.37e+003 Hz)

The voltage PI compensator theoretically produces infinite gain at DC. As a result, a zero steady-state voltage error can be achieved. The proportional gain is tuned to achieve the desired crossover frequency.

The current compensator nullifies the effect of the complex dominant poles (ω_{p1}), thereby simplifying the design of the outer voltage loop compensator (G_{cv}).

The general form of a PI compensator in continuous domain is given in Equation 18.

EQUATION 18: OUTER VOLTAGE LOOP PI COMPENSATOR ($G_{cv}(s)$) TRANSFER FUNCTION

$$G_{cv}(s) = K_p + \frac{K_i}{s} = \frac{K_{cv}(s + \omega_v)}{s}$$

Where:
K_p = Proportional Gain
K_i = Integral Gain
K_{cv} = Gain of PI Compensator
ω_v = Magnitude of PI Compensator Zero in Radians/Second

The desired crossover frequency is f_{cv} in Hz and $\omega_{cv} = j2\pi f_{cv}$ in radians/second. At crossover frequency, the loop gain of the system should be 0 dB or one in linear scale, as provided in Equation 19. The magnitude of $G_{cv}(s)$ is calculated by excluding K_{cv}.

EQUATION 19: COMPENSATOR GAIN CALCULATION
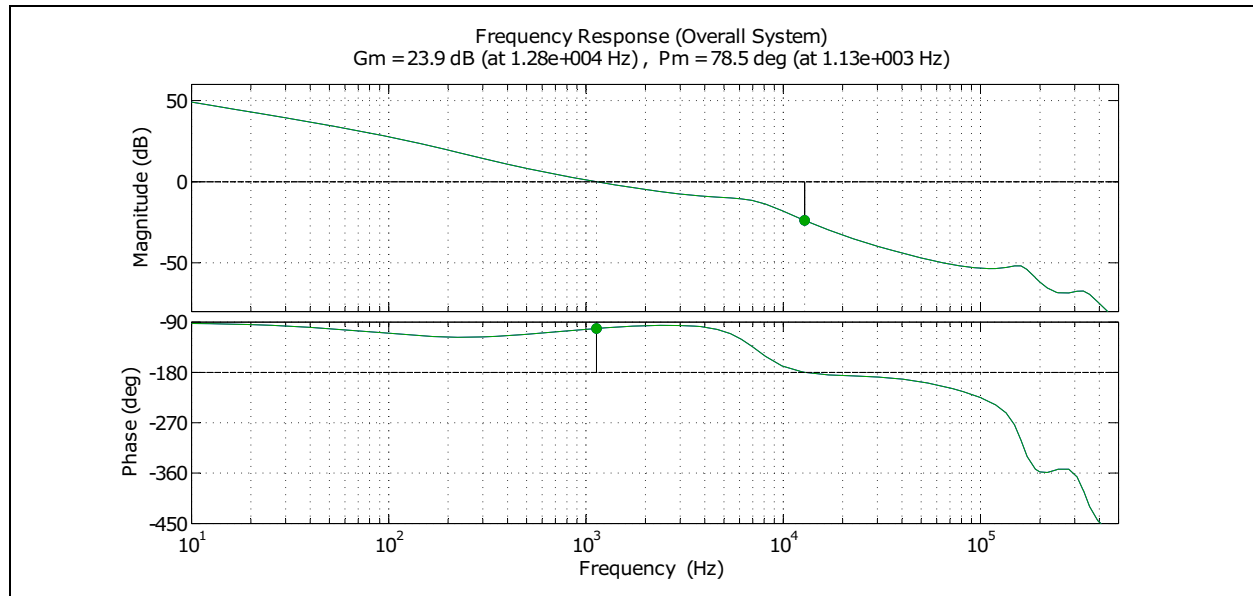
$$G_{vl}(s)\big|_{s = \omega_{cv}} \times G_{cv}(s)\big|_{s = \omega_{cv}} = 1$$

The Required Gain of the Compensator is:

$$K_{cv} = \frac{1}{G_{vl}(s)\big|_{s = \omega_{ci}} \times G_{cv}(s)\big|_{s = \omega_{cv}}}$$

The PI compensator zero (ω_v) is placed at 2500 radians/second to obtain the required phase at a crossover frequency of ~1 kHz, as provided in Equation 20.

EQUATION 20: COMPENSATOR TRANSFER FUNCTION ($G_{cv}(s)$)

$$G_{cv}(s) = \frac{4.9075(s + 2500)}{s} = \frac{4.907s + 1.227e004}{s}$$

The compensated converter loop gain ($G_{vs}(s)$) transfer function is provided in Equation 21.

EQUATION 21: CONVERTER LOOP GAIN ($G_{vs}(s)$)

Converter Loop Gain:

$$G_{vs}(s) = G_{fv}(s) \times G_{cv}(s) \times G_{delay}(s) \times G_{iCL}(s) \times G_{vi}(s)$$

The frequency response is illustrated in Figure 9.

FIGURE 9: CONVERTER LOOP GAIN

Frequency Response (Overall System)
Gm = 23.9 dB (at 1.28e+004 Hz), Pm = 78.5 deg (at 1.13e+003 Hz)

AN1495

Simulation results in Figure 9 indicate that the crossover frequency of the converter is at 1 kHz.

Figure 10 illustrates the measured loop gain obtained from the network analyzer. The measured crossover frequency of the converter is very close to 1 kHz, thereby confirming the model prediction.

FIGURE 10:   MEASURED LOOP GAIN OF THE CONVERTER
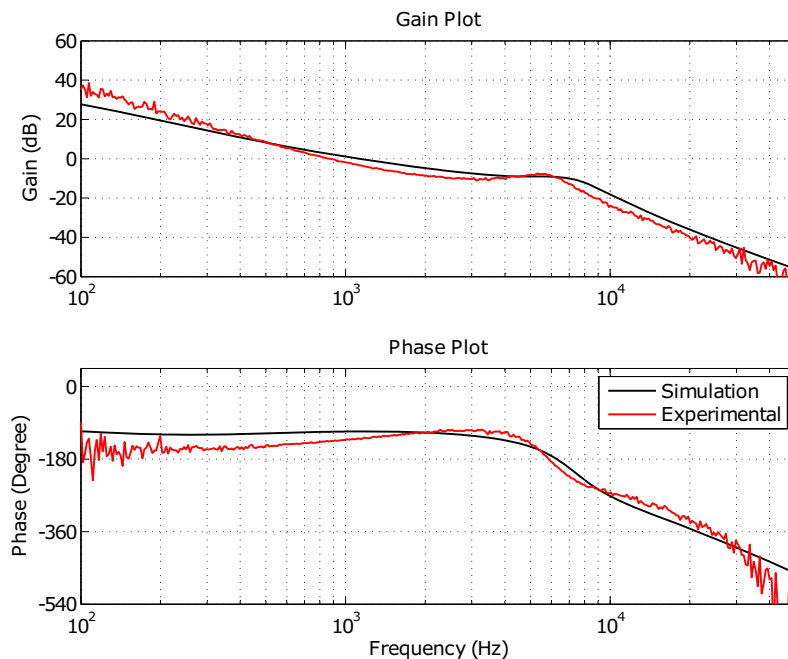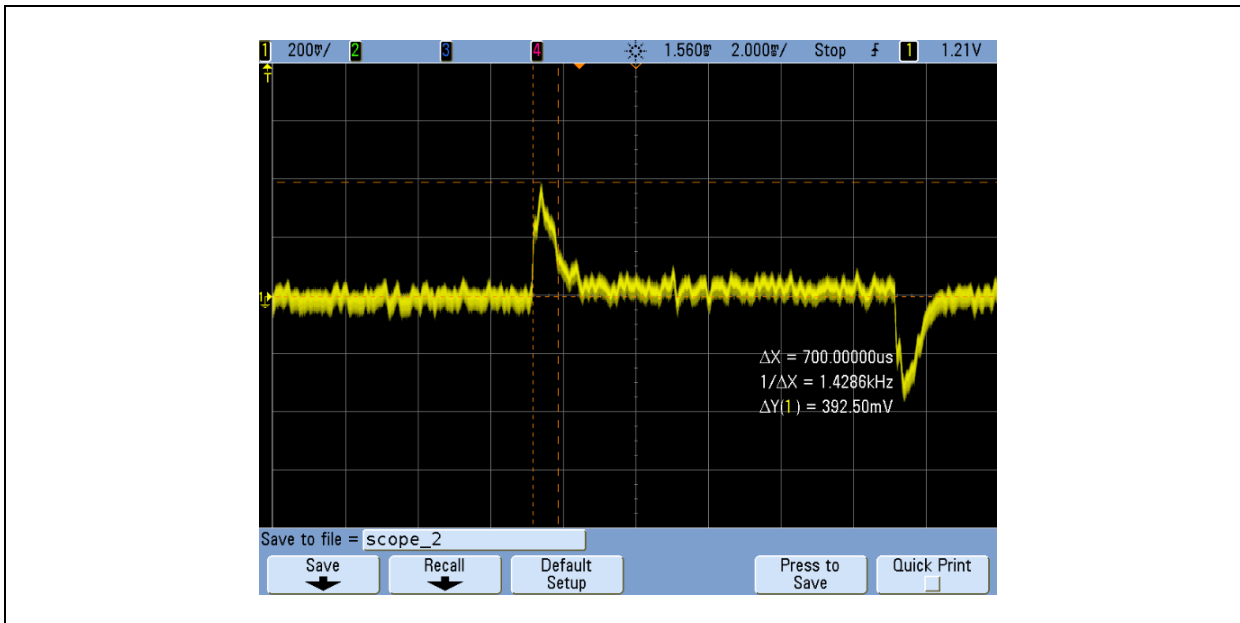
Figure 11 shows the load transient response of the Average Current Mode Controlled LLC converter. The load transient test is done from 25% to 75% load change. Overshoot and settling time are also shown in Figure 11.

FIGURE 11: MEASURED LOAD TRANSIENT RESPONSE OF THE CONVERTER

CONCLUSION

Average Current Mode Controlled (ACMC) Pulse-Frequency Modulated (PFM) LLC resonant converter plant transfer function is derived by employing Extended Describing Functions (EDF). The ACMC-LLC resonant converter has superior noise immunity, and provides good dynamic response and current sharing requirements of parallel connected converters. A multiloop digital compensator is designed to meet the specifications of phase margin, gain margin and bandwidth for the converter. The hardware results or waveforms are in conformity to the developed analytical model and also meet the target specifications.

REFERENCES

- *AN1477, "Digital Compensator Design for LLC Resonant Converter"* (DS00001477)
- *"Small-Signal Modeling of Series and Parallel Resonant Converters"*, by Yang E.X; Lee F.C; Jovanovich M.M, Applied Power Electronics Conference and Exposition, 1992. APEC' 92. Conference Proceedings 1992, Seventh Annual,1992, Page(s): 785-792
- *"Approximate Small-Signal Analysis of the Series and the Parallel Resonant Converters"*, by Voperian V, Power Electronics, IEEE Transactions on, Vol. 4, Issue 1, January 1989, Page(s): 15-24
- *AN1336, "DC/DC LLC Reference Design Using the dsPIC® DSC"* (DS01336)

LIST OF PARAMETERS

TABLE 1:   LIST OF PARAMETERS AND DESCRIPTION

Parameter	Description
V_{ref}	Reference output voltage
G_{cv}	Transfer function of voltage loop compensator
G_{delay}	Transfer functions of transportation delay
I_{ref}	Reference current
G_{ci}	Transfer function of the current loop compensator
$G_{v\omega}$	Transfer function between output voltage and switching frequency
$G_{i\omega}$	Transfer functions between inductor current and switching frequency
G_{fv}	Voltage measurement low-pass filter
G_{fc}	Current measurement low-pass filter
G_{vl}	Transfer function between output voltage and inductor current
K_p	Proportional gain of PI compensator
K_i	Integral gain of PI compensator
K_{cv}	Gain of outer voltage loop PI compensator
K_{ci}	Gain of 2P2Z compensator
i_r	Resonant inductor current
ω_s	Switching frequency
V_0	Output voltage
$K_{A/D}$	Gain of ADC measurement
TF	Transfer function

Note the following details of the code protection feature on Microchip devices:

- Microchip products meet the specification contained in their particular Microchip Data Sheet.

- Microchip believes that its family of products is one of the most secure families of its kind on the market today, when used in the intended manner and under normal conditions.

- There are dishonest and possibly illegal methods used to breach the code protection feature. All of these methods, to our knowledge, require using the Microchip products in a manner outside the operating specifications contained in Microchip's Data Sheets. Most likely, the person doing so is engaged in theft of intellectual property.

- Microchip is willing to work with the customer who is concerned about the integrity of their code.

- Neither Microchip nor any other semiconductor manufacturer can guarantee the security of their code. Code protection does not mean that we are guaranteeing the product as "unbreakable."

Code protection is constantly evolving. We at Microchip are committed to continuously improving the code protection features of our products. Attempts to break Microchip's code protection feature may be a violation of the Digital Millennium Copyright Act. If such acts allow unauthorized access to your software or other copyrighted work, you may have a right to sue for relief under that Act.

Trademarks

Worldwide Sales and Service

AMERICAS

Corporate Office
2355 West Chandler Blvd.
Chandler, AZ 85224-6199
Tel: 480-792-7200
Fax: 480-792-7277
Technical Support:
http://www.microchip.com/
support
Web Address:
www.microchip.com

Atlanta
Duluth, GA
Tel: 678-957-9614
Fax: 678-957-1455

Austin, TX
Tel: 512-257-3370

Boston
Westborough, MA
Tel: 774-760-0087
Fax: 774-760-0088

Chicago
Itasca, IL
Tel: 630-285-0071
Fax: 630-285-0075

Dallas
Addison, TX
Tel: 972-818-7423
Fax: 972-818-2924

Detroit
Novi, MI
Tel: 248-848-4000

Houston, TX
Tel: 281-894-5983

Indianapolis
Noblesville, IN
Tel: 317-773-8323
Fax: 317-773-5453
Tel: 317-536-2380

Los Angeles
Mission Viejo, CA
Tel: 949-462-9523
Fax: 949-462-9608
Tel: 951-273-7800

Raleigh, NC
Tel: 919-844-7510

New York, NY
Tel: 631-435-6000

San Jose, CA
Tel: 408-735-9110
Tel: 408-436-4270

Canada - Toronto
Tel: 905-695-1980
Fax: 905-695-2078

ASIA/PACIFIC

Australia - Sydney
Tel: 61-2-9868-6733

China - Beijing
Tel: 86-10-8569-7000

China - Chengdu
Tel: 86-28-8665-5511

China - Chongqing
Tel: 86-23-8980-9588

China - Dongguan
Tel: 86-769-8702-9880

China - Guangzhou
Tel: 86-20-8755-8029

China - Hangzhou
Tel: 86-571-8792-8115

China - Hong Kong SAR
Tel: 852-2943-5100

China - Nanjing
Tel: 86-25-8473-2460

China - Qingdao
Tel: 86-532-8502-7355

China - Shanghai
Tel: 86-21-3326-8000

China - Shenyang
Tel: 86-24-2334-2829

China - Shenzhen
Tel: 86-755-8864-2200

China - Suzhou
Tel: 86-186-6233-1526

China - Wuhan
Tel: 86-27-5980-5300

China - Xian
Tel: 86-29-8833-7252

China - Xiamen
Tel: 86-592-2388138

China - Zhuhai
Tel: 86-756-3210040

ASIA/PACIFIC

India - Bangalore
Tel: 91-80-3090-4444

India - New Delhi
Tel: 91-11-4160-8631

India - Pune
Tel: 91-20-4121-0141

Japan - Osaka
Tel: 81-6-6152-7160

Japan - Tokyo
Tel: 81-3-6880- 3770

Korea - Daegu
Tel: 82-53-744-4301

Korea - Seoul
Tel: 82-2-554-7200

Malaysia - Kuala Lumpur
Tel: 60-3-7651-7906

Malaysia - Penang
Tel: 60-4-227-8870

Philippines - Manila
Tel: 63-2-634-9065

Singapore
Tel: 65-6334-8870

Taiwan - Hsin Chu
Tel: 886-3-577-8366

Taiwan - Kaohsiung
Tel: 886-7-213-7830

Taiwan - Taipei
Tel: 886-2-2508-8600

Thailand - Bangkok
Tel: 66-2-694-1351

Vietnam - Ho Chi Minh
Tel: 84-28-5448-2100

EUROPE

Austria - Wels
Tel: 43-7242-2244-39
Fax: 43-7242-2244-393

Denmark - Copenhagen
Tel: 45-4450-2828
Fax: 45-4485-2829

Finland - Espoo
Tel: 358-9-4520-820

France - Paris
Tel: 33-1-69-53-63-20
Fax: 33-1-69-30-90-79

Germany - Garching
Tel: 49-8931-9700

Germany - Haan
Tel: 49-2129-3766400

Germany - Heilbronn
Tel: 49-7131-72400

Germany - Karlsruhe
Tel: 49-721-625370

Germany - Munich
Tel: 49-89-627-144-0
Fax: 49-89-627-144-44

Germany - Rosenheim
Tel: 49-8031-354-560

Israel - Ra'anana
Tel: 972-9-744-7705

Italy - Milan
Tel: 39-0331-742611
Fax: 39-0331-466781

Italy - Padova
Tel: 39-049-7625286

Netherlands - Drunen
Tel: 31-416-690399
Fax: 31-416-690340

Norway - Trondheim
Tel: 47-7288-4388

Poland - Warsaw
Tel: 48-22-3325737

Romania - Bucharest
Tel: 40-21-407-87-50

Spain - Madrid
Tel: 34-91-708-08-90
Fax: 34-91-708-08-91

Sweden - Gothenberg
Tel: 46-31-704-60-40

Sweden - Stockholm
Tel: 46-8-5090-4654

UK - Wokingham
Tel: 44-118-921-5800
Fax: 44-118-921-5820